

<https://doi.org/>

## **An analytical approach to reconstruction of axisymmetric defects in pipelines using T(0,1) guided waves\***

Yihui Da<sup>1</sup>, Bin Wang<sup>1</sup>, Dianzi Liu<sup>2,†</sup>, Zhenghua Qian<sup>1,†</sup>

1. State Key Laboratory of Mechanics and Control of Mechanical Structures, College of Aerospace Engineering, Nanjing University of Aeronautics and Astronautics, Nanjing, China

2. School of Engineering, University of East Anglia, Norwich, UK, NR4 7TJ

(Received Feb. 25, 2020/ Revised Jul. 11, 2020)

**Abstract** Torsional guided waves have been widely utilized to inspect surface corrosion in pipelines due to their simple displacement behavior and the ability of long-range transmission. Especially, the torsional mode T(0,1), which is the first order of torsional guided waves, plays the irreplaceable position and role, mainly because of its non-dispersion characteristic property. However, one of the most pressing challenges faced in modern quality inspection is to detect surface defects in pipelines with a high level of accuracy. Taking into account this situation, a quantitative reconstruction method using the torsional guided wave T(0,1) is proposed in this paper. The methodology for defect reconstruction consists of three steps. Firstly, reflection coefficients of the guided wave T(0,1) scattered by different sizes of axisymmetric defects are calculated using the developed hybrid finite element method (HFEM). Then, applying the boundary integral equation and Born approximation, Fourier transform of the surface defect profile can be analytically derived as the correlative product of reflection coefficients of torsional guided wave T(0,1) and the fundamental solution of the intact pipeline in frequency domain. Finally, reconstruction of defects is precisely performed by inverse Fourier transform of the product in the frequency domain. Numerical experiments show that the proposed approach is suitable for the detection of surface defects with arbitrary shapes. Meanwhile, effects of the depth and width of surface defects on the accuracy of defect reconstruction have been investigated. It is noted that the reconstructive error is less than 10%, providing the defect depth is no more than half of the pipe thickness.

**Key words** torsional guided wave, hybrid finite element method, boundary integral equation, quantitative reconstruction

**Chinese Library Classification O343**

**2010 Mathematics Subject Classification** 74J05, 74J20, 74J25

---

\* Citation: Da, Y., Wang, B., and Liu, D. An analytical approach to reconstruction of axisymmetric defects in pipelines using T(0,1) guided waves. *Applied Mathematics and Mechanics (English Edition)* (2020)

† Corresponding authors, E-mail: dianzi.liu@uea.ac.uk (D. Liu), qianzh@nuaa.edu.cn (Z. Qian)

©Shanghai University and Springer-Verlag GmbH Germany, part of Springer Nature 2020

## 1 Introduction

Pipelines, playing a significant role in the transportation of gases and liquids, usually expose in the natural environment for a long time and withstand corrosion from changes of the natural environment. Performance degradation of pipelines will undoubtedly affect normal operation and cause serious accidents like explosions and leakages. In order to check the working state of pipelines, many researchers have proposed various effective methods, by which defects have been successfully detected<sup>[1-8]</sup>.

Ultrasonic inspection, as an effective and nondestructive evaluation method, has been applied to structural health monitoring and damage detection. According to the properties of elastic waves, ultrasonic inspection mainly includes bulk waves inspection<sup>[9-12]</sup>, guided waves inspection<sup>[13-17]</sup>, and nonlinear ultrasonic inspection<sup>[18-21]</sup>. Due to the non-dispersion characteristics, guided waves inspection<sup>[22]</sup> has a unique advantage over other methods for testing large structures and it is a promising method for detecting long-distance transportation pipelines. However, the interaction between guided waves of pipelines and defects is very complicated, and analytical solution of Green's function, which is of great importance to reconstruct defects in pipelines, has still not been found. In 1958, Gazis studied the propagation of free harmonic waves along a hollow circular cylinder<sup>[23-24]</sup> as well as the plane-strain vibration of thick-walled hollow cylinders<sup>[25]</sup>. In these articles, Bessel functions and Hankel functions were used, and the approximate numerical solution of guided waves was found for hollow circular cylinders. Meitzler<sup>[26]</sup> and Zemanek<sup>[27]</sup> denoted modes of guided waves propagating along axial direction were denoted with 'L(0, m)', 'T(0, m)' and 'F(n, m)' where 'n' and 'm' indicate circumferential modes and axial modes respectively. L(0, m) and T(0, m) denote longitudinal modes and torsional modes of axisymmetric guided waves, and F(n, m) means flexural modes of non-axisymmetric guided waves which are much more complicated.

Meanwhile, the finite element method (FEM) was utilized for the analysis of propagation waves and edge vibrations in anisotropic composite cylinders by Huang and Dong<sup>[28]</sup>. Based on the same principle, Rattanawangcharoen et al.<sup>[29]</sup> adopted 2D FEM to solve reflection and transmission coefficients of axisymmetric guided waves in jointed laminated cylinders, and Bai et al.<sup>[1]</sup> analyzed scattered fields of circumferential cracks in pipes for symmetry and anti-symmetry of structures using semi-analytical finite element (SAFE), which is able to effectively calculate forward problems of elastic waves in pipes. With SAFE, singularities' discrepancies between no-flaw and flaw pipes proposed by Stoyko et al.<sup>[30]</sup> were used to detect and describe a notch in a pipe. In real experiments, James et al.<sup>[13]</sup> introduced an experimental platform for the construction of pipe models and obtained scattering signals of vary modes successfully. Similarly, an effective approach<sup>[31]</sup> for the excitation and propagation of torsional T(0,1) wave mode for detecting defects in a steel pipe by using finite element numerical simulations and experimental studies. A new two-dimensional localization algorithm based on the combination of detection theory and array processing is proposed to extract locations of multi-damage in a plate-like structure for structural health monitoring purpose<sup>[32]</sup>. The compressed sensing method for guided wave inspection is suggested to solve the problem of huge amounts of data and to maintain defect identification accuracy<sup>[33]</sup>.

Generally, most inspection methods need a large number of experimental data as reference values and have no ability to describe geometric shape of defects for a large region. However, the method of boundary integral equation (BIE) considers the scattered fields of incident waves and is capable of reconstructing defects. Kitahara et al.<sup>[9]</sup> investigated two inverse scattering methods based on body waves to reconstruct the shape of flaws in the elastic solid, and Wang et al.<sup>[34-36]</sup> adopted guided waves

of scattered waves to reconstruct geometric properties of surface flaws and internal flaws in plates. The reflective method can be applied successfully to monitor structural health in industrial pipelines based on a single permanently installed source–receiver pair<sup>[37]</sup>. Though many efforts were devoted to defect detection, this method has not been applied to quantitatively reconstruct defects in pipelines using guided waves.

In this paper, quantitative reconstruction of axisymmetric surface defects in pipelines has been proposed using BIE technique. The methodology for analytical defect detection mainly consists of three parts. In the first part, an integrated method of 3D FEM with semi-analytical finite element (SAFE)<sup>[38-39]</sup>, called Hybrid FEM (HFEM), is developed to solve the forward problem – determination of wave fields dependence on material and defect properties. Using HFEM, calculations of scattered fields for axisymmetric defects with different sizes are performed and reflection coefficients are obtained as functions of incident wave frequencies. Following that, the energy conservation principle is applied to verify the results obtained by HFEM. In the second part, the torsional mode  $T(0,1)$  of the guided wave is chosen to investigate the inverse problem – reconstruction of defects. Since Green’s function for the displacement field of  $T(0,1)$  propagating in pipelines is linearly proportional to the radius of pipes, the integral equation of the defect boundary is derived using the reciprocity theorem. Then, Born approximation and the far-field solution of Green’s function in pipelines are applied to the integral equation to investigate the relationship between the defect depth and reflection coefficients. Finally, the defect depth is analytically obtained by Fourier transform of reflection coefficients in frequency domain. In order to demonstrate the correctness and accuracy of the proposed reconstruction method, three numerical examples including a single rectangular defect, a double rectangular defect and a double-stepped defect, are examined. Results show the location and shape of defects can be efficiently and precisely identified. Moreover, effects of the defect depth and width on the accuracy of the reconstruction are analyzed. It is noted that the reconstruction error of the defective structure becomes larger as the defect depth increases. When the defect depths are equal to  $0.1667h$ ,  $0.3333h$ ,  $0.50h$  and  $0.6667h$ , where  $h$  means the pipeline thickness, the reconstruction errors are increased by 1.5170%, 5.2453%, 10.2669% and 16.6218%, respectively. However, the construction error resulting from the increase of the defect width is less than 2% as the defect depth keeps constant.

## 2 Calculations of scattered fields in pipelines using hybrid FEM

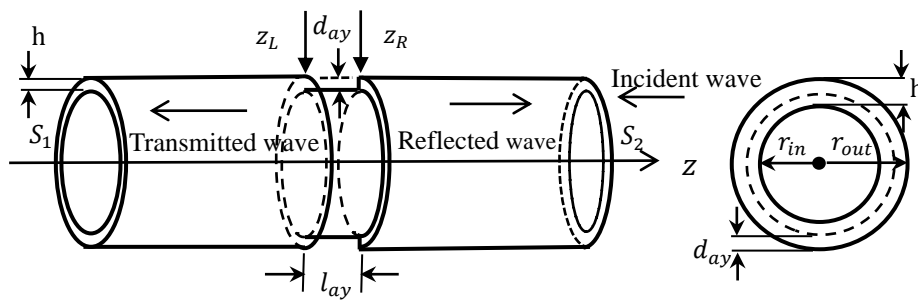


**Fig. 1** The diagram of a pipe with an axisymmetric defect.  $r_{in}$  and  $r_{out}$  represent inner and outer diameters,  $h$  is the wall thickness, and the width and depth of the axisymmetric defect are denoted as  $l_{ay}$  and  $d_{ay}$ , respectively. The truncated left and right cross sections are depicted as  $S_1$  and  $S_2$ . Coordinates for left and right edges of the defect are denoted as  $z_L$  and  $z_R$  in  $z$ -axis. The incident wave propagates along the negative  $z$ -axis direction.

The truncated part of a pipe including the defect has been modeled by 3D FEM shown in Fig.1 and the displacements and tractions on the  $S_1$  and  $S_2$  can be written as the summation of the expansion modes<sup>[30,39]</sup>, which is the principle of hybrid FEM used for solving the forward problem in this paper. Then, the equation of motion for an isotropic elastic medium is

$$\delta ([\mathbf{q}]^H) \mathbf{S} \mathbf{q} = \delta ([\mathbf{q}]^H) \mathbf{P} \quad (1)$$

where

$$\mathbf{S} = \mathbf{K} - \omega^2 \mathbf{M} \quad (2)$$

$\mathbf{K}$  and  $\mathbf{M}$  are global stiffness and mass matrices,  $\omega$  is a circular frequency,  $\mathbf{q}$  is a nodal displacement vector and  $\mathbf{P}$  is a nodal force vector. The superscript  $H$  represents conjugate transpose and  $\delta$  means the first variation. For the model of a pipeline structure shown in Fig. 1, all nodes are divided into two categories: one includes boundary nodes on cross sections  $S_1$  and  $S_2$ , which are indicated by the subscript B; the other contains interior nodes represented by the subscript I. Based on the previous work<sup>[40]</sup>, Eq. (1) can be rewritten as

$$[\mathbf{G}] \begin{bmatrix} \mathbf{q}_I \\ \tilde{\mathbf{A}} \end{bmatrix} = [\mathbf{T}] \quad (3)$$

$$\text{where } \mathbf{G} = \left\{ \begin{bmatrix} \mathbf{I} & \mathbf{0} \\ \mathbf{0} & [\tilde{\Phi}]^H \end{bmatrix} \begin{bmatrix} \mathbf{S}_{II} & \mathbf{S}_{IB} \\ \mathbf{S}_{BI} & \mathbf{S}_{BB} \end{bmatrix} \begin{bmatrix} \mathbf{I} & \mathbf{0} \\ \mathbf{0} & \tilde{\Phi} \end{bmatrix} - \begin{bmatrix} \mathbf{I} & \mathbf{0} \\ \mathbf{0} & [\tilde{\Phi}]^H \end{bmatrix} \begin{bmatrix} \mathbf{0} & \mathbf{0} \\ \mathbf{0} & \tilde{\mathbf{t}} \end{bmatrix} \right\},$$

$$\mathbf{T} = \begin{bmatrix} \mathbf{I} & \mathbf{0} \\ \mathbf{0} & [\tilde{\Phi}]^H \end{bmatrix} \left\{ \begin{bmatrix} \mathbf{0} \\ \tilde{\mathbf{t}}^1 \end{bmatrix} - \begin{bmatrix} \mathbf{S}_{II} & \mathbf{S}_{IB} \\ \mathbf{S}_{BI} & \mathbf{S}_{BB} \end{bmatrix} \begin{bmatrix} \mathbf{0} \\ \tilde{\Phi}^1 \end{bmatrix} \right\}, \quad \tilde{\mathbf{A}} = \begin{bmatrix} \tilde{A}_{01}^{\text{tra}} \\ \vdots \\ \tilde{A}_{0M}^{\text{tra}} \\ \tilde{A}_{01}^{\text{ref}} \\ \vdots \\ \tilde{A}_{0M}^{\text{ref}} \end{bmatrix}, \quad \tilde{\Phi} = [\tilde{\Phi}_{01}^{\text{tra}} \quad \dots \quad \tilde{\Phi}_{0M}^{\text{tra}} \quad \tilde{\Phi}_{01}^{\text{ref}} \quad \dots \quad \tilde{\Phi}_{0M}^{\text{ref}}],$$

$\tilde{\Phi}^1 = \begin{bmatrix} \tilde{\Phi}_{0m}^1 \\ \tilde{\Phi}_{0m}^2 \end{bmatrix}$ ,  $\tilde{\mathbf{t}}^1 = \begin{bmatrix} \mathbf{t}_{0m}^1 \\ \mathbf{t}_{0m}^2 \end{bmatrix}$ ,  $\tilde{\mathbf{t}} = [\tilde{\mathbf{t}}_{01}^{\text{tra}} \quad \dots \quad \tilde{\mathbf{t}}_{0M}^{\text{tra}} \quad \tilde{\mathbf{t}}_{01}^{\text{ref}} \quad \dots \quad \tilde{\mathbf{t}}_{0M}^{\text{ref}}]$ ,  $\mathbf{I}$  is an identity matrix,  $\mathbf{q}_I$  is the displacement vector of the interior nodes and  $\tilde{\mathbf{A}}$  is the modified coefficients for scattered fields.

Effects of the defect depth and width on reflection coefficients have been investigated using the developed HFEM. The material properties of the pipeline are shown as Table 1. For reconstruction of a single rectangular defect, a series of cases listed in Table 2 have been performed. Case 1 and Case 2 represent different defect depths and widths, respectively. To discover the dependence of the phase velocity on the wavelength, the dispersion relation of guided waves in pipeline structures has been shown in Fig. 2. Results indicate the relationship between the number of guided waves and the corresponding frequency as well as the displacement distribution of guided waves along the pipe thickness. Using HFEM, reflection coefficients of different guided waves shown in Fig. 3 and Fig. 4 have been calculated. It is noted that the reflection coefficients are defined as the ratio of incident displacements to reflected displacements for the same mode guided wave. In Fig. 3, the relationship between modes (L(0,1), L(0,2) and T(0,1)) of incident guided waves and the corresponding absolute values of the reflected coefficients has been demonstrated. When the defect length keeps constant (for example,  $d_{ay}=0.568h$ ), the absolute values of the reflected coefficients of all the guided waves become larger as the defect depths increase. When the defect depth remains constant, the similar conclusion can be drawn in Fig. 4. Therefore, either the depth or the length of the defect increases, which leads to the larger absolute values of reflected coefficients. Obviously, variations in defect depth have more impact on reflection coefficients of torsional guided waves in pipelines than those in defect length.

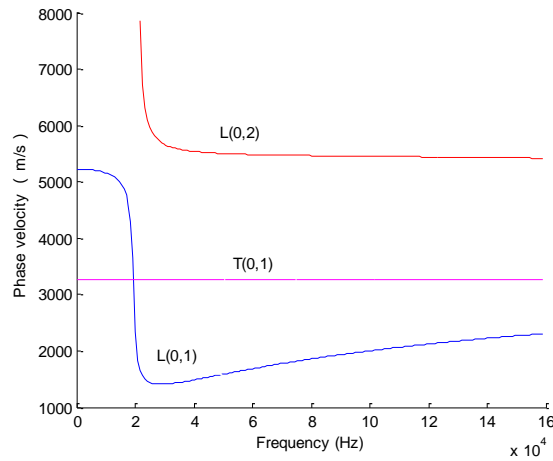
To demonstrate the relation between the defect profile and reflection coefficients for complex defects in pipelines, the analytical derivation of the relation will be provided in the following section.

**Table 1** Material properties of the pipe model

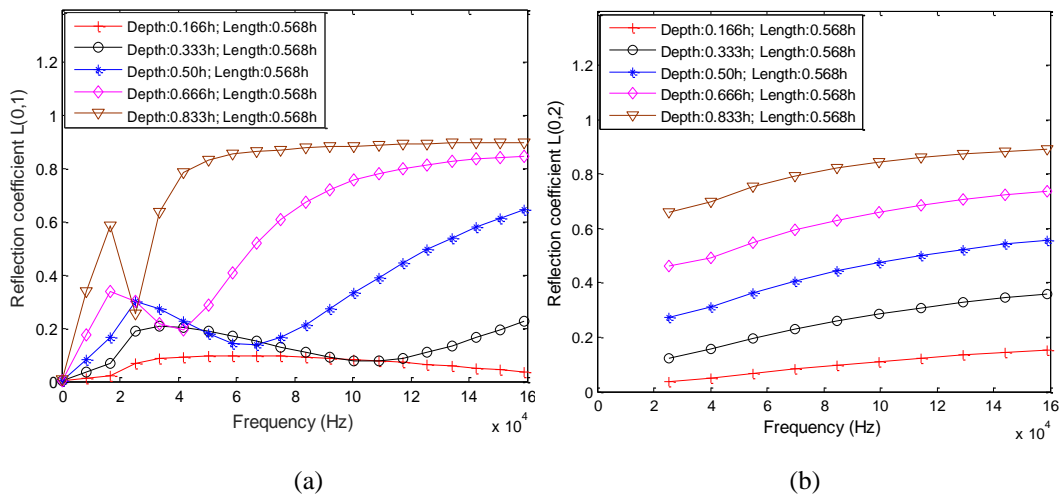
Density ( $\rho$ , kg/m <sup>3</sup> )	Inner radius ( $r_{in}$ , m)	Outer radius ( $r_{out}$ , m)	Wall thickness ( $h = r_{out} - r_{in}$ , m)	Lame constants ( $\lambda$ and $\mu$ , Pa)
$7.932 \times 10^3$	$3.881 \times 10^{-2}$	$4.440 \times 10^{-2}$	$5.590 \times 10^{-3}$	$1.132 \times 10^{11}$ and $8.430 \times 10^{10}$

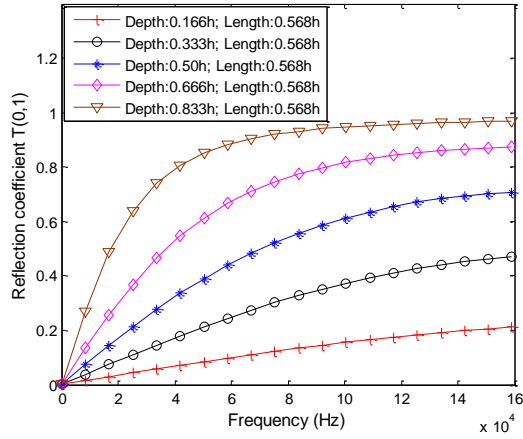
**Table 2** The statement of defects' size. In case 1 the defect depth  $d_{ay}$  is from 0.166h to 0.833h and the defect width  $l_{ay}$  equals to 0.568h; in case 2 the defect width is from 0.189h to 0.947h and the defect depth equals to 0.50h. h is thickness of the pipeline

Case 1	$d_{ay}$	0.166h	0.333h	0.50h	0.666h	0.833h
	$l_{ay}$	0.568h	0.568h	0.568h	0.568h	0.568h
Case 2	$d_{ay}$	0.50h	0.50h	0.50h	0.50h	0.50h
	$l_{ay}$	0.189h	0.379h	0.568h	0.757h	0.947h



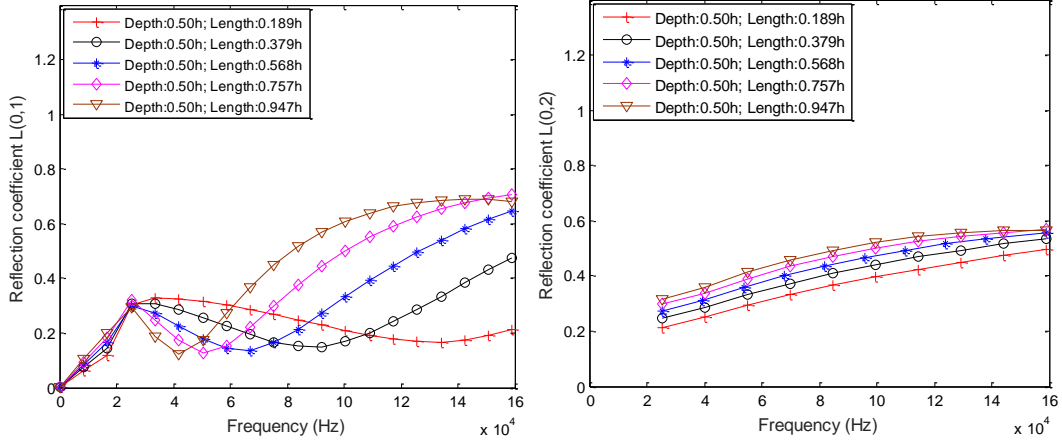
**Fig. 2** Dispersion relations of the guided waves L(0,1), L(0,2) and T(0,1) in pipelines





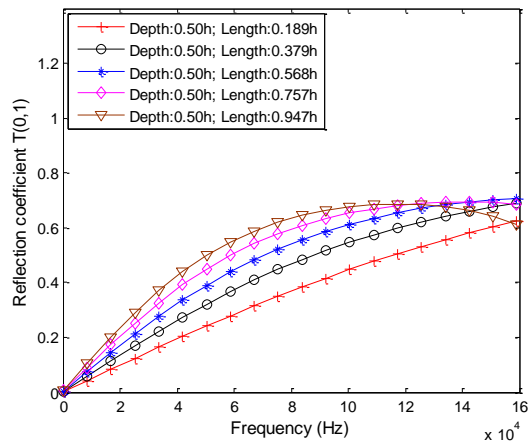
(c)

**Fig. 3** Absolute values of reflected coefficients of different guided waves varying with depth of the defects, when the defect width (length) identically equals to  $0.568h$ : (a)  $L(0,1)$ , (b)  $L(0,2)$ , (c)  $T(0,1)$



(a)

(b)



(c)

**Fig. 4** Absolute values of reflected coefficients of different guided waves varying with width (length) of the defects, when the defect depth identically equals to  $0.50h$ : (a)  $L(0,1)$ , (b)  $L(0,2)$ , (c)  $T(0,1)$

### 3 Analytical formulations for reconstruction of defects in pipelines

Wave fields in pipelines satisfy the Sommerfeld radiation conditions<sup>[41]</sup>, thus boundary integral equations (BIE) of the incident waves can be formulated as Eq. (4)

$$\int_S [\mathbf{u}^{inc}(\mathbf{x})\mathbf{T}(\mathbf{x} - \mathbf{X}) - \mathbf{p}^{inc}(\mathbf{x})\mathbf{U}(\mathbf{x} - \mathbf{X})]dS(\mathbf{x}) = \begin{cases} 0 & \mathbf{X} \notin V \\ -\mathbf{u}^{inc}(\mathbf{X})/2 & \mathbf{X} \text{ on } S \\ -\mathbf{u}^{inc}(\mathbf{X}) & \mathbf{X} \in V \end{cases} \quad (4)$$

where the time harmonic term  $e^{-i\omega t}$  is omitted;  $\mathbf{x}$  and  $\mathbf{X}$  represent the field point and source point, respectively; and  $\mathbf{u}^{inc}(\mathbf{x})$  and  $\mathbf{p}^{inc}$  is the displacement and traction of the incident guided wave on closed surface  $S$  of the defect  $V$ . This equation states  $\mathbf{U}(\mathbf{x} - \mathbf{X})$  and  $\mathbf{T}(\mathbf{x} - \mathbf{X})$  must be the displacement and traction of the fundamental solution to the current intact pipeline problem. Therefore, boundary integral equations of the scattered waves can be written in a form as Eq. (5)

$$\int_S [\mathbf{u}^{sca}(\mathbf{x})\mathbf{T}(\mathbf{x} - \mathbf{X}) - \mathbf{p}^{sca}(\mathbf{x})\mathbf{U}(\mathbf{x} - \mathbf{X})]dS(\mathbf{x}) = \begin{cases} \mathbf{u}^{sca}(\mathbf{X}) & \mathbf{X} \notin V \\ \mathbf{u}^{sca}(\mathbf{X})/2 & \mathbf{X} \text{ on } S \\ 0 & \mathbf{X} \in V \end{cases} \quad (5)$$

$\mathbf{u}^{sca}(\mathbf{x})$  and  $\mathbf{p}^{sca}(\mathbf{x})$  means displacement and traction of scattered waves on surface  $S$ . Although the incident guided wave only contains T(0,1), in the inverse problem the scattered waves are rather complex, especially near the defect region.

Adding Eqs. (4) and (5) we obtain

$$\int_S [\mathbf{u}^{tot}(\mathbf{x})\mathbf{T}(\mathbf{x} - \mathbf{X}) - \mathbf{p}^{tot}(\mathbf{x})\mathbf{U}(\mathbf{x} - \mathbf{X})]dS(\mathbf{x}) = \begin{cases} \mathbf{u}^{sca}(\mathbf{X}) & \mathbf{X} \notin V \\ (\mathbf{u}^{sca}(\mathbf{X}) - \mathbf{u}^{inc}(\mathbf{X}))/2 & \mathbf{X} \text{ on } S \\ -\mathbf{u}^{inc}(\mathbf{X}) & \mathbf{X} \in V \end{cases} \quad (6)$$

Where the total displacement  $\mathbf{u}^{tot}(\mathbf{x}) = \mathbf{u}^{inc}(\mathbf{x}) + \mathbf{u}^{sca}(\mathbf{x})$ , and the total traction  $\mathbf{p}^{tot}(\mathbf{x}) = \mathbf{p}^{inc}(\mathbf{x}) + \mathbf{p}^{sca}(\mathbf{x})$ .

For  $\mathbf{X} \notin V$ , Eq. (6) can be further simplified due to the free boundary condition  $\mathbf{p}^{tot}(\mathbf{x}) = 0$ ,

$$\int_S \mathbf{u}^{tot}(\mathbf{x})\mathbf{T}(\mathbf{x} - \mathbf{X})dS(\mathbf{x}) = \mathbf{u}^{sca}(\mathbf{X}) \quad \mathbf{X} \notin V \quad (7)$$

Generally, the defect depth is much less than wall thickness of pipelines. Therefore, a weak scattering source is assumed and  $\mathbf{u}^{tot}(\mathbf{x})$  is replaced by  $\mathbf{u}^{inc}$  using Born approximation<sup>[34]</sup>. Then, one has

$$\int_S \mathbf{u}^{inc}(\mathbf{x})\mathbf{T}(\mathbf{x} - \mathbf{X})dS(\mathbf{x}) \approx \mathbf{u}^{sca}(\mathbf{X}) \quad \mathbf{X} \notin V \quad (8)$$

Taking into account the relationship between the traction and the stress on the surface  $S$ , the traction of the fundamental solution satisfies

$$T_j^m(\mathbf{x} - \mathbf{X}) = \sigma_{ij}^m(\mathbf{x} - \mathbf{X})n_j(\mathbf{x}); i = j = m = 1,2,3 \quad (9)$$

where  $n_j$  is components of the normal vector of the surface  $S$ . Subscripts  $i, j$  and  $m$  represent three directions of  $r, \theta$ , and  $z$  in the cylindrical coordinate system. The superscript  $m$  represents the direction of body force acting at the source point  $\mathbf{X}$ . It is noted that for all of the equations, we adopt Einstein's summation convention.

Substituting Eq. (9) into Eq. (8), one has

$$\int_S u_i^{inc}(\mathbf{x})\sigma_{ij}^m(\mathbf{x} - \mathbf{X})n_j(\mathbf{x})dS(\mathbf{x}) \approx u_m^{sca}(\mathbf{X}) \quad \mathbf{X} \notin V \quad (10)$$

Furthermore, Eq. (11) can be obtained by applying the divergence theorem to Eq. (10) as follows,

$$\int_V \nabla_j [u_i^{inc}(\mathbf{x}) \sigma_{ij}^m(\mathbf{x} - \mathbf{X})] dV(\mathbf{x}) \approx u_m^{sca}(\mathbf{X}) = u_m^{ref}(\mathbf{X}) \quad \mathbf{X} \notin V \quad (11)$$

where  $(\nabla_1, \nabla_2, \nabla_3) = \left( \frac{\partial}{\partial r} + \frac{1}{r}, \frac{1}{r} \frac{\partial}{\partial \theta}, \frac{\partial}{\partial z} \right)$ .

Using the discrete nodal displacement  $\mathbf{q}^{inc}$  along the thickness, the displacement  $\mathbf{u}^{inc}(\mathbf{x})$  can be written in a function as  $\mathbf{u}^{inc}(\mathbf{x}) = \mathbf{N}\mathbf{q}^{inc}$ , where  $\mathbf{N}$  is the shape function, and the details can be referred to SAFE<sup>[38]</sup>. It is obvious that  $\mathbf{u}^{inc}(\mathbf{x})$  is a piecewise function and cannot be directly substituted into Eq. (11) for analytical derivation. However, the displacement induced by the torsional wave T(0,1) is proportional to the pipeline radius  $r$  and can be obtained by numerical fitting technique, one can have

$$u_1^{inc}(\mathbf{x}) = u_3^{inc}(\mathbf{x}) = 0; \quad u_2^{inc}(\mathbf{x}) = C_{0T_1}(k_{0T_1}) r e^{-ik_{0T_1}z} \quad (12)$$

where  $C_{0T_1}(k_{0T_1})$  is defined as the fitting coefficient, which is only dependent on wave numbers; and  $k_{0T_1}$  is wavenumber of T(0,1).

Applying the boundary conditions, stress components of fundamental solution can be written as

$$\begin{aligned} \sigma_{11}^2 = \sigma_{22}^2 = \sigma_{33}^2 = 0; \quad \sigma_{12}^2 = \sigma_{21}^2 = \sigma_{13}^2 = \sigma_{31}^2 = 0 \\ \sigma_{23}^2 = \sigma_{32}^2 = -ik_{0T_1} \mu C_{0T_1}(k_{0T_1}) r e^{-ik_{0T_1}(z-z_0)} \end{aligned} \quad (13)$$

where  $z_0$  is the z-axis coordinate of the source point,  $\mu$  is shear modulus. Thus, the integrand on the left side of Eq. (11) is simplified as

$$\nabla_j [u_i^{inc}(\mathbf{x}) \sigma_{ij}^m(\mathbf{x} - \mathbf{X})] = \frac{\partial}{\partial z} (u_2^{inc} \sigma_{23}^2) \quad (14)$$

Furthermore, the displacement field of reflected waves can also be denoted as

$$u_2^{ref}(\mathbf{x}) = R_{0T_1}^{ref} \text{conj}[C_{0T_1}(k_{0T_1}) r e^{-ik_{0T_1}z_0}] \quad (15)$$

$\text{conj}[\ ]$  represents conjugate transform and  $R_{0T_1}^{ref}$  means reflection coefficient. Substituting Eqs. (12) –

(15) into Eq. (11), one has

$$\int_{-\infty}^{+\infty} \int_{r_1}^{r_2} 2\pi (-2k_{0T_1}^2 C_{0T_1}^2 r^3) e^{-2ik_{0T_1}z} dr dz \approx R_{0T_1}^{ref} \text{conj}[C_{0T_1} r_{out}] \quad (16)$$

where  $r_{out}$  is the outer radius.

For a pipeline with surface axisymmetric defects, it is assumed that the depth of the defect is a function of  $z$ , and the integration bounds along the radial direction in Eq. (16) are determined by  $r_1 = r_{out} - d_{ay}(z)$  and  $r_2 = r_{out}$ , where  $d_{ay}(z)$  is the defect depth function. Hence, one has

$$\int_{-\infty}^{+\infty} \left( r^4 \Big|_{r_{out}-d_{ay}(z)}^{r_{out}} \right) e^{-2ik_{0T_1}z} dz \approx \frac{R_{0T_1}^{ref} \text{conj}[C_{0T_1} r_{out}]}{(-\pi k_{0T_1}^2 C_{0T_1}^2)} \quad (17)$$

where  $r^4 \Big|_{r_{out}-d_{ay}(z)}^{r_{out}} = 4r_{out}^3 d_{ay}(z) - 6r_{out}^2 [d_{ay}(z)]^2 + 12r_{out} [d_{ay}(z)]^3 - 12[d_{ay}(z)]^4$ . If

$d_{ay}(z) \ll h$ ,  $r^4 \Big|_{r_{out}-d_{ay}(z)}^{r_{out}} \approx 4r_{out}^3 d_{ay}(z)$  is obtained. Therefore, Eq. (17) can be rewritten as

$$\int_{-\infty}^{+\infty} d_{ay}(z) e^{-2ik_{0T_1}z} dz \approx \frac{R_{0T_1}^{ref} \text{conj}[C_{0T_1} r_{out}]}{4r_{out}^3 (-\pi k_{0T_1}^2 C_{0T_1}^2)} \quad (18)$$

Assuming  $\frac{R_{0T_1}^{ref} \text{conj}[c_{0T_1} r_{out}]}{4r_{out}^3 (-\pi k_{0T_1}^2 c_{0T_1}^2)} = D_{ay}(2k_{0T_1})$ , Eq. (18) is a standard Fourier transform formula. Its

inverse transformation is given by

$$d_{ay}(z) = \frac{1}{2\pi} \int_{-\infty}^{+\infty} D_{ay}(2k_{0T_1}) e^{2ik_{0T_1}z} d(2k_{0T_1}) \quad (19)$$

To solve  $d_{ay}(z)$  by IFFT (Inverse Fast Fourier Transform) technique, the longitudinal resolution ratio ( $\Delta z$ ) of defect reconstruction should satisfy the equation  $\Delta z = \frac{\pi}{2\text{Max}|k_{0T_1}|}$ . In order to clearly reconstruct, the single-rectangular defect,  $\Delta z \leq l_{ay}/4$ , which implies that  $\text{Max}|k_{0T_1}|$  must be greater than  $2\pi/(l_{ay})$ . It is certain that much higher resolution ratio is required for reconstruction of the defect with a complex shape.

#### 4 Numerical experiments for defect reconstruction

In this section, HFEM simulations and analytical analysis for reconstruction of defects have been examined by three examples including (a) a single-rectangular defect; (b) a step-structure defect; (c) a double-rectangular defect. The reconstructive results have been shown in Fig. 5 (a), (b) and (c), respectively. The frequency range of the incident wave in this research has been selected from  $9.2817 \times 10^2 \text{Hz}$  to  $6.4972 \times 10^5 \text{Hz}$ . Based on dispersion characteristics of torsional guided wave modes shown in Fig. 6, three modes of T(0,1), T(0,2) and T(0,3) could be generated by continuously exciting ultrasonic waves along the circumference. Possessing the constant phase velocity, the torsional guided wave T(0,1) is selected as the incident wave. Using HFEM, reflection coefficients of the guided wave T(0,1) propagating in three defective pipelines shown in Fig. 5 have been represented in Figs. 7(a), 8(a) and 9(a), respectively. The correctness of simulations is proved by conservation of energy during the reflection and transmission of torsional guided waves. It is obvious that the summation of transmission energy and reflection energy in Figs. 7(b), 8(b) and 9(b) is equal to one.

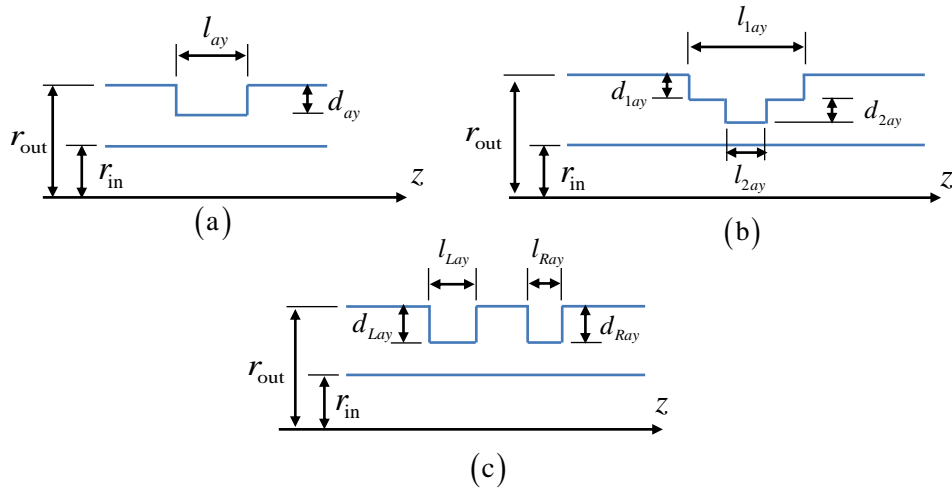


**Fig. 5** Pipe profiles with three types of defects: (a) single-rectangular defect, the depth  $d_{ay} = 9.317 \times 10^{-4} \text{m}$  and width  $l_{ay} = 5.698 \times 10^{-3} \text{m}$ ; (b) stepped-defect, the depths  $d_{1ay} = d_{2ay} = 4.657 \times 10^{-4} \text{m}$ , and the widths  $l_{1ay} = 1.252 \times 10^{-2} \text{m}$  and  $l_{2ay} = 4.696 \times 10^{-3} \text{m}$ ; (c) double-rectangular defect, the depths  $d_{Lay} = d_{Ray} = 9.317 \times 10^{-4} \text{m}$ , and the

widths  $l_{Lay} = 7.189 \times 10^{-3} \text{m}$  and  $l_{Ray} = 4.790 \times 10^{-3} \text{m}$ . The inner and outer radius of the pipes are denoted as  $r_{in} = 3.881 \times 10^{-2} \text{m}$  and  $r_{out} = 4.440 \times 10^{-2} \text{m}$

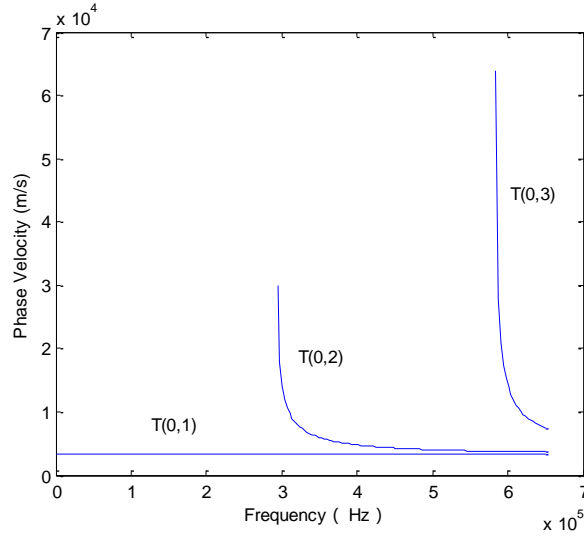


**Fig. 6** Dispersion characteristics of torsional guided wave modes in pipes

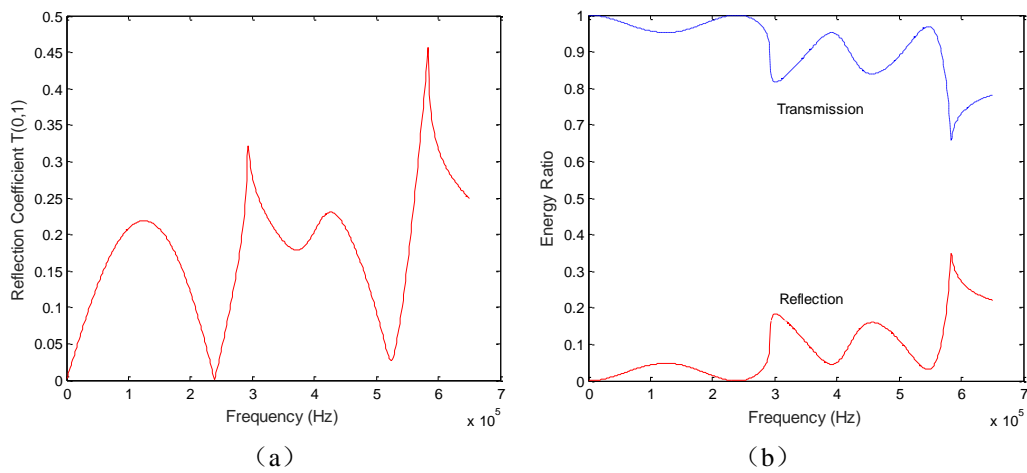


**Fig. 7** The numerical results of reflection guided wave T(0,1) for the single-rectangular defect: (a) reflection coefficients of T(0,1); (b) transmission energy and reflection energy

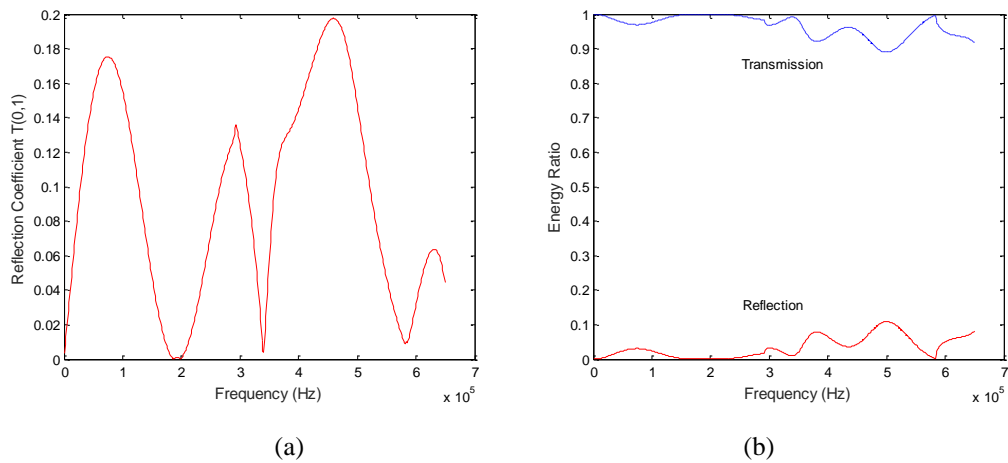


**Fig. 8** The numerical results of reflection guided wave T(0,1) for the stepped-defect: (a) reflection

coefficients of  $T(0,1)$ ; (b) transmission energy and reflection energy

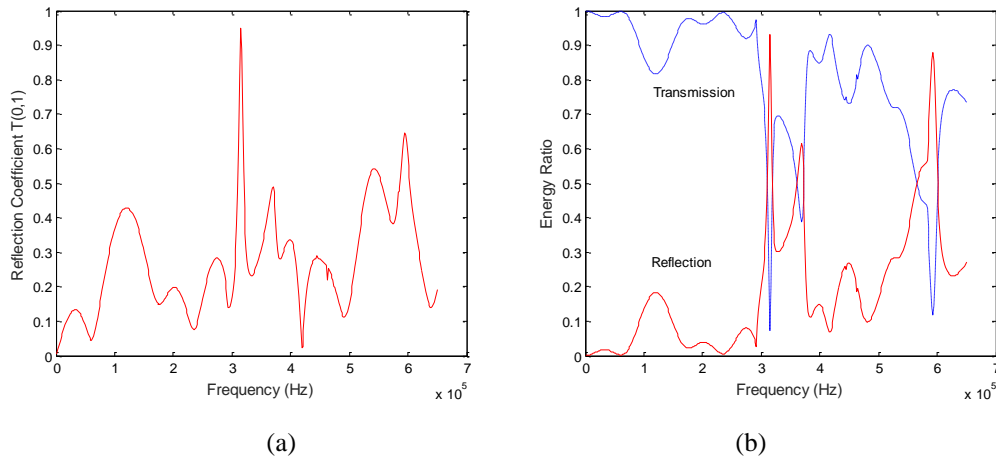


**Fig. 9** The numerical results of reflection guided wave  $T(0,1)$  for the double-rectangular defect: (a) reflection coefficients of  $T(0,1)$ ; (b) transmission energy and reflection energy

Applying IFFT (Inverse Fast Fourier Transform) technique, the depth functions of the defective pipelines can be analytically reconstructed using Eq. (19). Both the defect locations and profiles have been successfully obtained, which are shown in Figs. 10, 11 and 12. It is noted that the defect width can be precisely determined, for example, the step-structure defect shown in Fig. 11. In this paper, each defect profile has been effectively reconstructed by more than four sampling points (the red dots). However, from the single-defect case to the double-defect case, the reconstruction error increases as the number of defects becomes larger. To address this problem, future work on the feasible resolution ratio ( $\Delta z$ ) should be investigated. Meanwhile, the reconstruction of the transmission region (along the negative direction of  $z$ -axis) is worse than the result in the reflection region (along the positive direction of  $z$ -axis) due to the incident guided waves propagating along the negative of  $z$ -axis in all the numerical experiments. Therefore, the Root Mean Square Error (RMSE) criterion is adopted to improve the accuracy of constructive results in this paper.

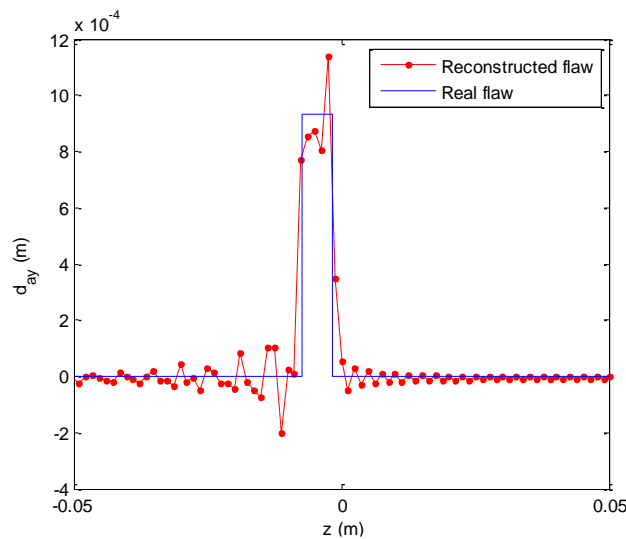


**Fig. 10** Reconstruction result of the single-rectangular defect

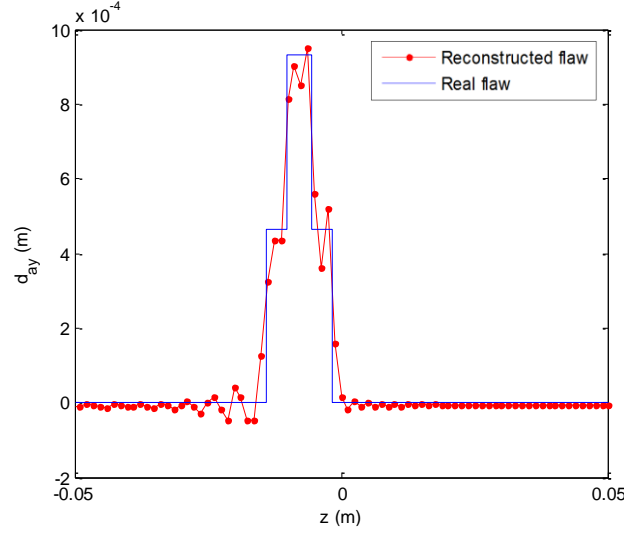


**Fig. 11** Reconstruction result of the step-structure defect

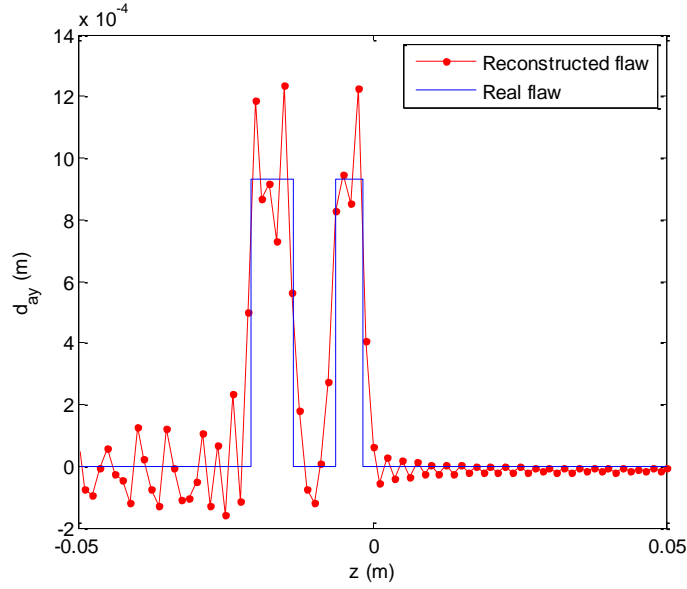


**Fig. 12** Reconstruction result of the double-rectangular defect

Numerical simulations and analytical analysis performed in the above three examples have demonstrated the capability of the developed method for reconstruction of different types of defect profiles. However, the assumption of Born approximation shown in Eq. (8) has restrained the defect size at the level of a shallow or surface scale. Therefore, it is necessary to investigate the effect of the defect size on the accuracy of defect reconstruction. In this research, the root mean square error (RMSE) criterion has been used to evaluate the difference between the reconstruction result and the real defect. The formulation of RMSE can be written as

$$\text{RMSE} = \frac{1}{h} \sqrt{\frac{\sum_{i=1}^N (d_i - \tilde{d}_i)^2}{N}} \quad (20)$$

where  $h$  means the wall thickness of a pipeline,  $N$  is the number of the sampling points to represent the defect geometry, and  $d_i$  and  $\tilde{d}_i$  mean the real defect depth and reconstruction depth, respectively.

For different defect sizes, errors between the reconstruction results and the real defects have been

given in Table 3. The wall thickness ( $h$ ) of a pipeline is 0.0056m. When the defect depth equals to 0.167 times the thickness, i.e.  $9.319 \times 10^{-4}$ m, the error is 1.517%. As the defect depth increases to one half of the thickness, i.e.  $2.80 \times 10^{-3}$ m, the error reaches up to 10.267%. Furthermore, when the defect depth is 0.667 times the thickness, i.e.  $3.727 \times 10^{-3}$ m, the error is increased by approximately 16.622%. However, when the defect width decreases, the reconstruction error increases. This is because the increase of the defect width results in the resolution enhancement for the given frequency interval of incident guided waves. Summarily, the shallower the defect depth becomes, the wider the defect width appears, and the smaller the reconstruction error is.

**Table 3** The reconstruction errors for different sizes of rectangular defects. The first column and row indicate defect depth and defect width

Defect width(m) \ Defect depth (m)	$4.347 \times 10^{-3}$	$7.826 \times 10^{-3}$	$1.131 \times 10^{-2}$	$1.478 \times 10^{-2}$
$9.319 \times 10^{-4}$	1.517%	1.084%	1.116%	1.106%
$1.863 \times 10^{-3}$	5.245%	4.594%	3.731%	3.498%
$2.80 \times 10^{-3}$	10.267%	9.592%	8.122%	7.959%
$3.727 \times 10^{-3}$	16.622%	16.187%	15.087%	15.268%

## 5 Conclusions

In this paper, an efficient and analytical reconstruction method for surface axisymmetrical defects in pipelines is proposed. The hybrid FEM has been applied to solve the forward problem to calculate the reflection coefficients and SAFE has been used to obtain the analytical far-field fundamental solution of the torsional guided wave  $T(0,1)$  propagating in the pipeline structure. The analytical defect depth function has been formulated by Fourier transform of the product of the reflection coefficients and the far-field fundamental solution. Three numerical detection experiments for different defect shapes have been performed to demonstrate the accuracy of the developed method for reconstruction of defects in terms of the location and profile of the defect. It is concluded that the reconstruction profile in the reflection region of guided waves has been more precisely reconstructed than the result in the transmission region, which sheds light on the demand of sensor placements located in the reflection region of guided waves for receiving signals. Results show that the reconstruction accuracy is more sensitive to the defect depth than the defect width. The deeper the defect depth becomes, the larger the reconstruction error is. However, when the depth is less than the half of the wall thickness of the pipeline, the reconstruction error is no more than 10.3%, which demonstrates the proposed method with a high level of accuracy. As most surface defects in pipelines have been mainly caused by corrosion, the defect thinning is usually far less than the half of the thickness. Based on this observation, reconstruction precision of the developed approach is sufficient to justify engineering requirements. Therefore, the quantitative defect detection in this paper is a significant and effective ultrasonic non-destructive evaluation method applicable to a wide range of industrial processes.

**Acknowledgements** This work was supported in part by the State Key Laboratory of Mechanics and Control of Mechanical Structures at NUAU [Grant number MCMS-E-0520K02], in part by the Key Laboratory of impact and Safety Engineering, Ministry of Education, Ningbo University [CJ201904], in part by the National Natural Science Foundation of China [Grant numbers 11502108, 1611530686].

**References**

- [1] BAI, H., SHAH, A. H., POPPLEWELL, N., and DATTA, S. K. Scattering of guided waves by circumferential cracks in composite cylinders. *International Journal of Solids and Structures*, **39**(17), 4583-4603 (2002) [https://doi.org/10.1016/S0020-7683\(02\)00339-6](https://doi.org/10.1016/S0020-7683(02)00339-6)
- [2] HAY, T. R. and ROSE, J. L. Flexible PVDF comb transducers for excitation of axisymmetric guided waves in pipe. *Sensors and Actuators A Physical*, **100**(1), 18-23 (2002) [https://doi.org/10.1016/S0924-4247\(02\)00044-4](https://doi.org/10.1016/S0924-4247(02)00044-4)
- [3] NURMALIA, NAKAMURA, N., OGI, H., and HIRAO, M. EMAT pipe inspection technique using higher mode torsional guided wave T(0,2). *NDT and E International*, **87**, 78-84 (2017) <https://doi.org/10.1016/j.ndteint.2017.01.009>
- [4] VINOGRADOV, S., EASON, T., and LOZEV, M. Evaluation of magnetostrictive transducers for guided wave monitoring of pressurized pipe at 200 °C. *Journal of Pressure Vessel Technology*, **140**(2), 021603 (2018) <https://doi.org/10.1115/1.4038726>
- [5] HEINLEIN, S., CAWLEY, P., and VOGT, T. K. Reflection of torsional T(0,1) guided waves from defects in pipe bends. *NDT and E International*, **93**, 57-63 (2018) <https://doi.org/10.1016/j.ndteint.2017.09.007>
- [6] GHAVAMIAN, A., MUSTAPHA, F., BAHARUDIN, B. T. H. T., and YIDRIS, N. Detection, localisation and assessment of defects in pipes using guided wave techniques: A review. *Sensors*, **18**(12), 4470 (2018) <https://doi.org/10.3390/s18124470>
- [7] HU, C. and XU, J. Center frequency shift in pipe inspection using magnetostrictive guided waves. *Sensors and Actuators: A. Physical*, **298**, 111583 (2019) <https://doi.org/10.1016/j.sna.2019.111583>
- [8] NAKHLI MAHAL, H., YANG, K., and NANDI, A. Defect detection using power spectrum of torsional waves in guided-wave inspection of pipelines. *Applied Sciences*, **9**(7), 1-24 (2019) <https://doi.org/10.3390/app9071449>
- [9] KITAHARA, M., NAKAHATA, K., and HIROSE, S. Elastodynamic inversion for shape reconstruction and type classification of flaws. *Wave Motion*, **36**(4), 443-455 (2002) [https://doi.org/10.1016/S0165-2125\(02\)00035-5](https://doi.org/10.1016/S0165-2125(02)00035-5)
- [10] HIROSE, S. Inverse scattering for flaw type classification. *International Union of Theoretical and Applied Mechanics*, Springer, Berlin, Heidelberg (1993) [https://doi.org/10.1007/978-3-642-52439-4\\_35](https://doi.org/10.1007/978-3-642-52439-4_35)
- [11] FELICE, M. V. and FAN, Z. Sizing of flaws using ultrasonic bulk wave testing: A review. *Ultrasonics*, **88**, 26-42 (2018) <https://doi.org/10.1016/j.ultras.2018.03.003>
- [12] YI, D., PEI, C., LIU, T., and CHEN, Z. Inspection of cracks with focused angle beam laser ultrasonic wave. *Applied Acoustics*, **145**, 1-6 (2019) <https://doi.org/10.1016/j.apacoust.2018.09.012>
- [13] BARSHINGER, J., , ROSE, J. L., and AVIOLI, M. J., Jr. Guided wave resonance tuning for pipe inspection. *Journal of Pressure Vessel Technology*, **124**(3), 303-310 (2002) <https://doi.org/10.1115/1.1491580>
- [14] SHIN, H. J. and ROSE, J. L. Guided wave tuning principles for defect detection in tubing. *Journal of Nondestructive Evaluation*, **17**(1), 27-36 (1998) <https://doi.org/10.1023/A:1022680429232>
- [15] LOWE, M. J. S., ALLEYNE, D. N., and CAWLEY, P. Defect detection in pipes using guided waves. *Ultrasonics*, **36**(1-5), 147-154 (1998) [https://doi.org/10.1016/s0041-624x\(97\)00038-3](https://doi.org/10.1016/s0041-624x(97)00038-3)
- [16] PANDA, R. S., RAJAGOPAL, P., and BALASUBRAMANIAM, K. Rapid guided wave

- inspection of complex stiffened composite structural components using non-contact air-coupled ultrasound. *Composite Structures*, **206**, 247-260 (2018) <https://doi.org/10.1016/j.compstruct.2018.08.024>
- [17] CANTERO-CHINCHILLA, S., CHIACHÍO, J., CHIACHÍO, M., CHRONOPOULOS, D., and JONES, A. Optimal sensor configuration for ultrasonic guided-wave inspection based on value of information. *Mechanical Systems and Signal Processing*, **135**, 106377 (2020) <https://doi.org/10.1016/j.ymssp.2019.106377>
- [18] DONSKOY, D., SUTIN, A., and EKIMOV, A. Nonlinear acoustic interaction on contact interfaces and its use for nondestructive testing. *NDT and E International*, **34**(4), 231-238 (2001) [https://doi.org/10.1016/s0963-8695\(00\)00063-3](https://doi.org/10.1016/s0963-8695(00)00063-3)
- [19] JHANG, K. Y. Nonlinear ultrasonic techniques for nondestructive assessment of micro damage in material: A review. *International Journal of Precision Engineering and Manufacturing*, **10**, 123-135 (2009) <https://doi.org/10.1007/s12541-017-0018-3>
- [20] POTTER, J. and CROXFORD, A. J. Characterization of nonlinear ultrasonic diffuse energy imaging. *IEEE Transactions on Ultrasonics, Ferroelectrics, and Frequency Control*, **65**(5), 870-880 (2018) <https://doi.org/10.1109/tuffc.2018.2816243>
- [21] ANDREADES, C., MALFENSE FIERRO, G. P., MEO, M., and CIAMPA, F. Nonlinear ultrasonic inspection of smart carbon fibre reinforced plastic composites with embedded piezoelectric lead zirconate titanate transducers for space applications. *Journal of Intelligent Material Systems and Structures*, **30**(20), 2995-3007 (2019) <https://doi.org/10.1177/1045389x19873419>
- [22] ROSE, J. L. A baseline and vision of ultrasonic guided wave inspection potential. *Journal of pressure vessel technology*, **124**(3), 273-282 (2002) <https://doi.org/10.1115/1.1491272>
- [23] GAZIS, D. C. Three-dimensional investigation of the propagation of waves in hollow circular cylinders. I . Analytical foundation. *Journal of the Acoustical Society of America*, **31**(5), 568-573 (1959) <https://doi.org/10.1121/1.1907753>
- [24] GAZIS, D. C. Three-dimensional investigation of the propagation of waves in hollow circular cylinders. II . Numerical results. *Journal of the Acoustical Society of America*, **31**(5), 573-578 (1959) <https://doi.org/10.1121/1.1907754>
- [25] GAZIS, D. C. Exact analysis of the plane-strain vibrations of thick-walled hollow cylinders. *Journal of the Acoustical Society of America*, **31**(2), 250 (1959) <https://doi.org/10.1121/1.1907708>
- [26] MEITZLER, A. H. Mode coupling occurring in the propagation of elastic pulses in wires. *Journal of the Acoustical Society of America*, **33**(4), 435-445 (1961) <https://doi.org/10.1121/1.1908685>
- [27] ZEMANEK, J. An experimental and theoretical investigation of elastic wave propagation in a cylinder. *Journal of the Acoustical Society of America*, **51**(1B), 265-283 (1972) <https://doi.org/10.1121/1.1912838>
- [28] HUANG, K. H. and DONG, S. B. Propagating waves and edge vibrations in anisotropic composite cylinders. *Journal of Sound and Vibration*, **96**(3), 363-379 (1984) [https://doi.org/10.1016/0022-460X\(84\)90363-8](https://doi.org/10.1016/0022-460X(84)90363-8)
- [29] RATTANAWANGCHAROEN, N., ZHUANG, W., SHAH, A. H., and DATTA, S. K. Axisymmetric guided waves in jointed laminated cylinders. *Journal of Engineering Mechanics*, **123**, 1020-1026 (1997) [https://doi.org/10.1061/\(ASCE\)0733-9399\(1997\)123:10\(1020\)](https://doi.org/10.1061/(ASCE)0733-9399(1997)123:10(1020))
- [30] STOYKO, D. K., POPPLEWELL, N., and SHAH, A. H. Detecting and describing a notch in a

- pipe using singularities. *International Journal of Solids and Structures*, **51**(15-16), 2729-2743 (2014) <https://doi.org/10.1016/j.ijsolstr.2014.02.002>
- [31] NIU, X., DUAN, W., CHEN, H., and MARQUES, H. R. Excitation and propagation of torsional T(0,1) mode for guided wave testing of pipeline integrity. *Measurement*, **131**, 341-348 (2019) <https://doi.org/10.1016/j.measurement.2018.08.021>
- [32] BAHADOR, M. M., ZAIMBASHI, A., and RAHGOZAR, R. Three-stage Lamb-wave-based damage localization algorithm in plate-like structures for structural health monitoring applications. *Signal Processing*, **168**, 107360 (2020) <https://doi.org/10.1016/j.sigpro.2019.107360>
- [33] WANG, Z., HUANG, S., WANG, S., ZHUANG, S., WANG, Q., and ZHAO, W. Compressed sensing method for health monitoring of pipelines based on guided wave inspection. *IEEE Transactions on Instrumentation and Measurement*, **69**(7), 4722-4731 (2020) <https://doi.org/10.1109/TIM.2019.2951891>
- [34] WANG, B. and HIROSE, S. Inverse problem for shape reconstruction of plate-thinning by guided SH-waves. *Materials transactions*, **53**(10), 1782-1789 (2012) <https://doi.org/10.2320/matertrans.I-M2012823>
- [35] WANG, B. and HIROSE, S. Shape reconstruction of plate thinning using reflection coefficients of ultrasonic lamb waves: a numerical approach. *ISIJ International*, **52**(7), 1320-1327 (2012) <https://doi.org/10.2355/isijinternational.52.1320>
- [36] WANG, B., QIAN, Z., and HIROSE, S. Inverse shape reconstruction of inner cavities using guided SH-waves in a plate. *Shock and Vibration*, **2015**, 1-9 (2015) <https://doi.org/10.1155/2015/195682>
- [37] VOGELAAR, B., PRIEMS, G., BOURGONJE, K., and GOLOMBOK, M. Time-lapse acoustic monitoring of deteriorating pipes. *Structural Health Monitoring*, **18**(5-6), 1995-2003 (2019) [doi:10.1177/1475921718815422](https://doi.org/10.1177/1475921718815422)
- [38] ZHUANG, W. and SHAH, A. H. Elastodynamic green's function for laminated anisotropic circular cylinders. *Journal of Applied Mechanics*, **66**(3), 665-674 (1999) <https://doi.org/10.1115/1.2791535>
- [39] MARZANI, A. Time-transient response for ultrasonic guided waves propagating in damped cylinders. *International Journal of Solids and Structures*, **45**(25), 6347-6368 (2008) <https://doi.org/10.1016/j.ijsolstr.2008.07.028>
- [40] DA, Y., DONG, G., WANG, B., LIU, D., and QIAN, Z. A novel approach to surface defect detection. *International Journal of Engineering Science*, **133**, 181-195 (2018) <https://doi.org/10.1016/j.ijengsci.2018.09.005>
- [41] LESTER W. SCHMERR J. R. *Fundamentals of ultrasonic nondestructive evaluation*, Plenum Press, New York, 72-75 (1998)